Microporous and Mesoporous Materials 230 (2016) 66–75

Contents lists available at ScienceDirect

Microporous and Mesoporous Materials

journal homepage: www.elsevier.com/locate/micromeso

Sulfonic functionalized SBA-15 catalysts in the gas phase glycerol dehydration. Thermal stability and catalyst deactivation

B.O. Dalla Costa [a], M.S. Legnoverde [b], C. Lago [a], H.P. Decolatti [a], C.A. Querini [a, *]

[a] Instituto de Investigaciones en Catálisis y Petroquímica (INCAPE), FIQ, UNL, CONICET, Santiago del Estero 2654, Santa Fe, S3000AOJ, Argentina
[b] Centro de Investigación y Desarrollo en Ciencias Aplicadas (CINDECA), FCE, UNLP, CONICET, Calle 47 N° 257, La Plata, B1900AJK, Argentina

ARTICLE INFO

Article history:
Received 6 January 2016
Received in revised form
9 April 2016
Accepted 26 April 2016
Available online 27 April 2016

Keywords:
Glycerol dehydration
Sulfonic SBA-15
Thermal stability
Deactivation

ABSTRACT

The catalytic conversion of glycerol to acrolein was studied using sulfonic functionalized mesoporous silica SBA-15. The catalysts were prepared by the co-condensation method, conducting the silica synthesis and functionalization of its surface with thiol-propyl groups in the same stage. In a next step, the oxidation of thiol groups to sulfonic groups was made varying the concentration of H_2O_2 in order to obtain catalysts with different levels of acidity on the surface. The solids were characterized by BET, SEM, FTIR, XPS, and potentiometric titration with n-butilamine. The thermal stability was analyzed by thermogravimetry (TGA) and temperature-programmed desorption (TPD). The reaction tests were performed at different temperatures between 275 °C and 350 °C, and under feed flow conditions that allowed the study of the deactivation phenomena by coke deposition. The best temperature in order to maximize the acrolein yield was 300 °C. Higher temperatures led to a rapid deactivation by a combined effect of coke deposition and decomposition of functional groups.

1. Introduction

The reduced availability of fossil raw materials has motivated the chemical industries to search alternative feedstocks for the synthesis of value-added fuels, chemicals and materials. As one of the biomass-derived oxygenated hydrocarbons, glycerol is currently formed as a by-product during the synthesis of biodiesel, by the transesterification of triglyceride with methanol or ethanol [1]. Approximately, a volume equivalent to 10% of the volume of biodiesel produced consists of glycerol. Due to the increase in biodiesel production, it is predicted that by 2020, 2700 million tons of glycerol will be generated worldwide [2], all of which should be efficiently processed in order to improve the economics of the biodiesel sector. Crude glycerol, a low-cost feedstock, can be converted into value-added products by various catalytic processes [3–17]. An attractive possibility is the catalytic dehydration of glycerol to produce acrolein, being a chemical intermediate for the production of acrylic acid, methionine, superabsorbers, polymers and detergents [13]. Acrolein production process is currently carried out by partial oxidation of propylene, which is made from fossil fuel, using mixed metal oxides as catalysts [18]. Therefore, the use of glycerol as raw material for the synthesis of acrolein could be more economical and eco-friendly than using propylene [19,20].

Several solid acid catalysts have been studied in the gas phase dehydration of glycerol, such as metal phosphates [21–24], metal sulphates [25,26], metal oxides [20,27], supported metal oxides [28], heteropolyacids supported on metal oxides [29–31], hierarchical porous materials [32] and zeolites [33–36]. In terms of acidity, it has been reasonably established that Brønsted acid sites catalyzes acrolein production [34,35,37], whereas Lewis acid sites increases the selectivity to hydroxyacetone [28,38–40]. In addition to the acidity, the textural properties of the solids play an important role in this process [41,42], and catalysts with small pores showed lower activity than catalysts with mesopores ranged between 6 and 10 nm [35,43].

Several studies have demonstrated the effects of pore structures and acid properties on catalytic performance. In particular, mesoporous acidic catalysts with different acidic properties were used for the dehydration of glycerol. A comparison of these solids with microporous and mesoporous acid-catalysts verified the benefits of hierarchical pores on enhancing the apparent activity and stability of the catalyst, and also highlights that overall catalytic performance is determined by the combined action of porous and acidic properties.

* Corresponding author. Santiago del Estero 2654, 3000, Santa Fe, Argentina.
E-mail address: querini@fiq.unl.edu.ar (C.A. Querini).

http://dx.doi.org/10.1016/j.micromeso.2016.04.035
1387-1811/

Among the possible alternative mesoporous materials proposed to improve selectivity to acrolein, sulfonic functionalized SBA-15 catalysts have been reported to be active for different reactions such as alcohol coupling to ethers, acetylation of glycerol, condensation, esterification and transesterification reactions [44–51]. Ziarani et al. summarized an overview on the application of sulfonic acid functionalized SBA-15 in various organic reactions [52].

The surface functionalization can be made either by introducing mercaptopropyl groups onto the pore wall surface via a secondary modification route [53–56], or via the co-condensation route [57–63], incorporating functional groups during the preparation of the materials. The co-condensation method is advantageous because it allows a high degree of organic moieties dispersion and the incorporation of thermally-stable covalent Si–C anchoring bonds [44]. In all cases, the oxidation of mercapto to sulfonic groups is carried out with hydrogen peroxide.

The deactivation mechanism on SBA-15 catalysts has not been addressed in many papers. For example, Oliveira et al. [37] characterized the coke deposits on non-functionalized SBA-15 having low acidity.

In this work, the objective was to study the performance of sulfonic-functionalized SBA-15 catalysts prepared by the co-condensation route, in the gas phase dehydration of glycerol. The effect of different levels of acidity in the catalytic activity and stability was studied. Also the impact of different reaction parameters on the acrolein yield and catalyst stability was analyzed. The deactivation is particularly addressed, and its relationship with the acid sites density is analyzed. In addition, the SBA catalysts used in the present study have higher levels of acid sites density than previously reported investigations. Several characterization techniques were used to obtain information regarding the acidity, thermal stability and textural properties of the catalysts.

2. Experimental

2.1. Materials

A mixture of glycerol (99.5%, Cicarelli) and distilled water was used as feedstock for the activity tests. In the synthesis of silica-based mesostructured materials, the silica source used was tetraethylorthosilicate (TEOS, 98%, Aldrich), using a copolymer poly(ethyleneglycol)-*block*-poly(propyleneglycol)-*block*-poly(-ethyleneglycol) (PE-PP-PE Pluronic P123, Aldrich) as the structure-directing agent, in HCl (Baker) acid medium. Mercaptopropyltrimethoxysilane (MPTMS, 95%, Aldrich) was employed as precursor for the incorporation of the functional groups on the silica surface. The oxidation of thiol groups to sulfonic was carried out employing hydrogen peroxide in different concentrations (H_2O_2 30 vol%, 20 vol% and 10 vol%, Panreac).

2.2. Catalysts synthesis

The SBA-15 mesoporous silica was prepared according to the procedure described by Zhao et al. [64]. In a typical preparation, 4 g of Pluronic P123 block copolymer were dissolved in an aqueous solution of HCl (2 mol L^{-1}) with stirring at 35 °C. Then, TEOS was added drop by drop to the system and stirring was continued for 20 h. Subsequently the reacting mixture was heated to 80 °C for 24 h. The molar composition used was 1TEOS:5HCl:0.018-PEO:184H_2O. The solid material obtained was washed with water, dried at 120 °C and calcined for 6 h at 540 °C.

Surface modification of SBA-15 can be readily accomplished by all the methods developed for silica [59,65–67].

For the synthesis of SBA-15 containing sulfonic groups, the usual procedure is carried out in two steps. In the first step, mercapto groups are attached to the pore surface. The introduction of this surface group can be done either during the sol-gel reaction of hexagonal arrangement of mesopores (co-condensation) or by post-synthesis functionalization. In the second step, the mercapto group is oxidized to sulfonic group by H_2O_2 [68].

Nevertheless, some authors have attained the oxidation and grafting simultaneously [60]. Alternatively, it is also possible the attachment of sulfonic groups to the pre-bounded surface mercapto groups [69].

In this work, propyl-thiol mesoporous silica material was synthesized by co-condensation of TEOS and MPTMS, in the presence of P123 in HCl acid medium, employing the sol-gel technique (co-condensation). It was demonstrated in our previous work [49] that a complete oxidation of the mercapto groups is not achieved, but this method allows to obtain the higher concentration of sulfonic species. The H_2O_2 concentration is modified to obtain different concentration of oxidized species, and therefore different acid sites density.

The molar composition of each mixture for 4 g of copolymer was 1TEOS:0.11MPTMS:0.018PEO:6.5HCl:27.1H_2O. The resultant solution was stirred for 20 h at 40 °C, after which the mixture was aged at 80 °C for 70 h under static conditions. The solid product was recovered by filtration and air-dried at room-temperature overnight. The template was removed from the as-synthesized material by washing with ethanol under reflux for 24 h, employing 100 ml of ethanol per gram of material. After thiol functionalization, oxidation proceeded by soaking the resulting solid in an aqueous dissolution of hydrogen peroxide (H_2O_2 30 vol%), following the method described by Bossaert et al. [68]. After the oxidation treatment, the solution was filtered and the solid was washed with ethanol. The wet material was suspended (1 wt%) in H_2SO_4 solution (1 mol L^{-1}) for 2 h. The powder was then washed with water and ethanol and dried for 2 h at 120 °C.

Other two catalysts SBA-15(20) and SBA-15(10) were synthesized using the same method of preparation, but oxidizing with H_2O_2 20 vol% and 10 vol% respectively.

The functionalized samples were labeled SBA-15(X), where X denotes the concentration of H_2O_2, with X: 30, 20 and 10.

2.3. Catalysts characterization

The catalysts were characterized by SEM, XPS, FTIR, adsorption-desorption of N_2, and the acidity was analyzed by titrating with *n*-butylamine. The particles size and morphology were determined using SEM.

Nitrogen adsorption-desorption isotherms were measured at the temperature of liquid nitrogen (−196 °C) using a Micrometrics ASAP 2020 instrument. Before adsorption, samples were outgassed by heating at 100 °C in vacuum, with a pressure lower than 3×10^{-2} mm Hg during 12 h. The surface area was calculated according to the Brunauer–Emmett–Teller (BET) equation. The pore size was obtained by the BJH method. The pore volume was taken at the $P/P_0 = 0.989$ single point.

Scanning electron microscopy (SEM) was carried out on Philips 505 microscope. For these analyses a small amount of sample was placed on a carbon tape and then it was coated by sputtering with gold.

FT-IR spectra were collected by means of an FT-IR Spectrometer Spectrum 1000, Perkin Elmer, using KBr in the frequency range of 4000–400 cm^{-1}.

The XPS analyses were performed in a multi-technique system (SPECS) equipped with a dual Mg/Al X-ray source and a hemispherical PHOIBOS 150 analyzer operating in the fixed analyzer

transmission (FAT) mode. The spectra were obtained with pass energy of 30 eV and the Mg anode was operated at 200 W, for the analysis of the core level signals of O 1s, Si 2p, S 2p and C 1s and with a multi-channel detector. The working pressure in the analyzing chamber was lower than 2 10^{-8} mbar. The samples were mounted on a sample rod, placed in the pre-treatment chamber of the spectrometer, submitted to evacuation during 10 min at 120 °C, and then evacuated at ultra high vacuum for 2 h. The spectra were processed using the software CasaXPS (Casa Software Ltd, UK). The intensities were estimated by calculating the integral of each peak after subtracting a Shirley-type background and fitting the experimental curve to a combination of Lorentzian and Gaussian lines. Binding energy values were referred to the C1 peak (284.6 eV). For the quantification of the elements, sensitivity factors provided by the manufacturers were used.

The change in acidity due to functionalization was determined by potentiometric titration. A known mass of the solid to be analyzed was suspended in acetonitrile. The suspension was titrated using a solution of *n*-butylamine (0.1 mol L^{-1}) in acetonitrile at 0.05 ml min^{-1}. The electrode potential variation was recorded on a digital pH meter (Metrohm 794 Basic Titrino apparatus with a double junction electrode). This technique was also utilized for detecting acid sites in the deactivated catalysts, after the reaction.

2.4. Coke characterization

Coke deposited during the reaction was characterized by temperature-programmed oxidation (TPO). In these experiments a modified technique was employed [70] in which the gases coming out of the sample cell passed through a methanation reactor. A H_2 stream was fed to this reactor, which was loaded with a Ni catalyst, and quantitatively converted CO and CO_2 to CH_4. This compound was continuously measured using a flame ionization detector (FID). Under these methanation conditions (400 °C, carrier 5% O_2 in N_2 at 40 ml min^{-1}) a 100% conversion of COx was reached, and in this way the sensitivity of the technique was greatly improved. The analysis cell was loaded with approximately 10 mg of catalyst and the analyses were performed heating from 20 °C to 750 °C, at a rate of 12 °C min^{-1}. This specific heating rate was selected to minimize both energy transference limitations and sensibility problems. At very low heating rate, lower sensitivity is obtained, while at high heating rates, energy transference limitations occur [70]. The equipment was calibrated using pulses of CO_2 diluted in He.

2.5. Thermal stability studies

The thermal stability of the samples was studied by thermogravimetry (TGA), in a Netzsch STA 449F3 instrument. About 5 mg of sample was loaded into an alumina crucible and heated at 10° min^{-1}, from 20 °C to 700 °C, with a N_2 flow rate of 50 ml min^{-1}. From the TGA profiles, the differential thermal gravimetric profiles (DTG) were obtained.

The thermal stability of the functional groups in the samples was also studied by temperature-programmed desorption (TPD). These experiments were carried out in the same equipment than that used in the TPO experiments, with the same heating rate (12 °C min^{-1}), but using N_2 as carrier gas. The decomposition of the propyl chain and its subsequent methanation allowed the detection by FID.

2.6. Catalyst performance tests

The dehydration of glycerol was conducted at atmospheric pressure in a continuous fixed-bed reactor, using 0.2 g of catalyst. The reactor was placed in an electrically heated furnace with an inner diameter that matched the outer diameter of the reactor in order to optimize heat transfer, and provided with a temperature control system. Before each reaction, the catalyst was pre-treated at 200 °C in N_2 flow for 1 h. The feed was an aqueous solution containing 20 wt% glycerol, and was introduced in the system at different flow rates, in order to obtain the desired glycerol weight hourly space velocity (WHSV). For most reaction experiments, the WHSV in terms of glycerol was 3.5 h^{-1}, which was relatively high compared with the values (0.85 h^{-1}) reported for SBA-15 catalysts studied in this reaction [71]. The use of a high WHSV was selected in order to study the catalyst stability and the deactivation phenomena at different temperatures, although experiences at WHSV = 1 h^{-1} were also carried out.

The mixture glycerol-water was evaporated in a preheater at 260 °C, with 50 ml min^{-1} of N_2 as carrier gas. After the reaction, the carrier flow was maintained during 1 h, in order to purge the system.

Reaction products together with the unconverted glycerol were collected in a cold trap maintained at 5 °C at 30 min intervals. The analysis of the products was carried out offline on a Shimadzu gas chromatograph (GC) equipped with a Phenomenex ZB-Wax capillary column (30 m × 0.32 mm × 0.25 μm) and a flame ionization detector (FID). A volumetric method was employed to determine the concentration of glycerol in the collected samples [72]. The following equations were used to calculate conversion, product yield and selectivity:

$$\text{Glycerol conversion}\ (\%) = \frac{\text{mol of glycerol reacted}}{\text{mol of glycerol fed}} \text{ x } 100$$

$$\text{Product yield}\ (\%) = \frac{\text{mol of product}}{\nu.\ \text{mol of glycerol fed}} \text{ x } 100$$

$$\text{Product selectivity}\ (\%) = \frac{\text{product yield}}{\text{glycerol conversion}} \text{ x } 100$$

The coefficient ν represents the amount of matter (in mol) of a given product obtained per mol of glycerol, being 1.5 for acetaldehyde and 1 for all the others products.

3. Results and discussions

3.1. Catalysts characterization

3.1.1. Textural properties

Fig. 1A shows the N_2 adsorption–desorption isotherms that correspond to the SBA-15 and SBA-15(X) functionalized samples studied in this work. All samples exhibit type IV isotherms typical of mesoporous structures, with a H1 hysteresis loop, associated with capillary condensation in the mesopores [73].

The relationship between the adsorption increase at $P/P_0 < 0.4$ corresponding to the multilayer adsorption and the second increase at $P/P_0 = 0.4–0.7$, depends on the presence of functional groups. Additionally, functionalization leads to changes in the hysteresis loop. The capillary condensation step for the functionalized samples is closing down at lower P/P_0 values in comparison to the original SBA-15, being 0.40 for the former and 0.45 for the latter, what indicates that the pores are narrowed after functionalization.

The mesopores size distributions (Fig. 1B) were calculated using the thermodynamic-based Barret-Joyner-Halenda (BJH) method. The desorption branch of the isotherm was used for the SBA-15. The hysteresis loop for nitrogen isotherms of the functionalized SBA-15(X) closing near to 0.40–0.42 in relative pressure, indicates that the cavitation phenomenon can be present [74,75]. Hence, for

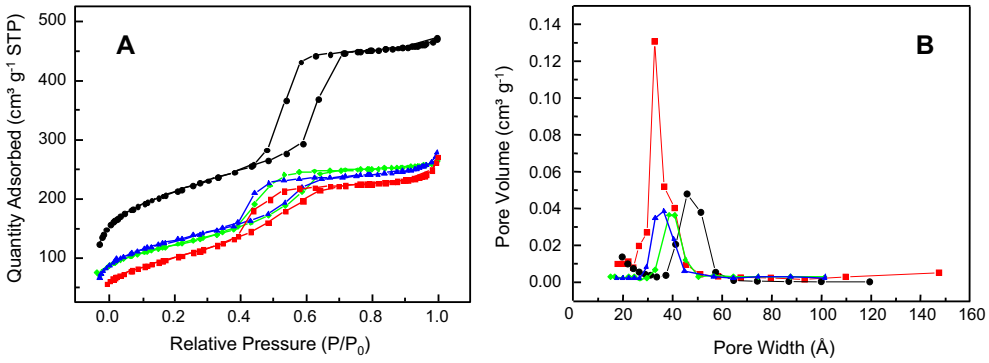

Fig. 1. **(A)** N_2 adsorption/desorption isotherms, **(B)** Pore size distribution; for samples SBA-15 (●), SBA-15(30) (■), SBA-15(20) (▲) and SBA-15(10) (♦).

these samples the adsorption branch was used to evaluate their pore size distribution.

The textural characteristics of these catalysts are summarized in Table 1. It is observed that the functionalization produces an important decrease of the surface area and a noticeable reduction of the pore volume as compared to the SBA-15. In addition to the functionalization of the surface, one of the possible causes of the decrease of the pore volume is that in the functionalized samples the completely removal of the template by washing with ethanol has not been achieved. This in turn is accomplished more efficiently in the SBA-15 sample by calcining. The reason why washing with ethanol is adopted after functionalization is associated with the thermal stability of the functional groups. It is assumed that during the outgassing at 100 °C under vacuum prior to the N_2 adsorption–desorption measurements, not all the template is removed in the SBA-15(X) samples.

The advantages of co-condensation method are high loading density of the organosilanes and the homogeneous distribution of the functional groups. However, one problem with this method is the extraction efficiency for the block copolymer systems which were only ca. 80% [76]. Nevertheless, although extraction is not as effective as calcination, differences in the textural properties cannot be attributed solely to the presence of template residues within the pores. XPS analyses were used to estimate the amount of template left in these catalysts, as discussed below.

3.1.2. Characterization by SEM

SEM images (Fig. 2A) reveal the typical form of SBA-15 particles as agglomerates with the form of wheat grains composed of small cylinders. SEM micrographs indicate that the presence of MPTS in the synthesis media do not alter the usual morphology presented by SBA-15 structure, but the size of these agglomerates is smaller in the functionalized sample SBA-15(30) (Fig. 2B). This can be explained considering that the morphologies depend on the evolution of the micelle shapes as a consequence of the interaction with the silicate [77], and MPTS interferes with this interaction. Similar results were observed for samples SBA-15(20) and SBA-15(10).

3.1.3. FTIR analysis

The FTIR analysis shows variations in the spectra caused by the organo-functionalization. Fig. 3 shows the spectra corresponding to the original sample SBA-15 and to the samples after functionalization. The spectrum that corresponds to the non-functionalized SBA-15 is equal to that reported by Oliveira et al. [37]. Asymmetric stretching vibrations of Si–O–Si at 1100 cm^{-1}, symmetric stretching vibrations from Si–O bonds at 800 cm^{-1} and bending vibrations from Si–O–Si at 466 cm^{-1} are clearly observed. The peak around 960 cm^{-1} corresponds to non-condensed Si–OH groups [78,79]. The broad band around 3400 cm^{-1} and the peak around 1630 cm^{-1} are due to the stretching and bending vibrations of adsorbed H_2O. The C–O–C vibrations (◆) at 1375 and 1456 cm^{-1} evidence the presence of rest of copolymer in the functionalized samples, being less visible these signals for the sample SBA-15(30). The absorption bands in the 1375 and 1456 cm^{-1} region are very small in the functionalized samples; however, these signals are not observed in the SBA-15(30) sample, supporting the idea of the presence of copolymer residues. The bands at 600 and 890 cm^{-1} are due to C–S (■) and S–O (▲) stretching vibrations, respectively [80]. A weak vibration corresponding to the SH group (●) is also observed at 2400 cm^{-1}, indicating the presence of non-oxidized groups. This signal is more appreciable for the samples SBA-15(20) and SBA-15(10), indicating differences in the degree of oxidation. These results also show that the concentration of H_2O_2 determines the fraction of SH groups that are oxidized, and consequently, of the final acidity of the catalyst. The bands at 2400 cm^{-1} could also correspond to the symmetric and asymmetric stretching of C–O bond in the CO_2 molecule. However, this compound adsorbs preferentially on basic materials and the signal was observed precisely on the acid functionalized catalysts, while it is not observed on the non-acidic SBA-15. In addition, the catalysts are treated under vacuum before the FTIR and it can be expected that the CO_2 be desorbed during this treatment.

3.1.4. XPS analysis

Surface chemical compositions of the synthesized samples were determined by XPS and results are shown in Table 2. As expected, the non-functionalized support SBA-15 has mainly silicon and

Table 1
Textural properties.

Sample	BET surface area(m^2 g^{-1})	Pore vol (cm^3 g^{-1}) at $P/P_0 = 0.99$	Pore size (Å)
SBA-15	750	0.72	48
SBA-15(30)	366	0.41	32
SBA-15(20)	423	0.47	37
SBA-15(10)	438	0.41	41

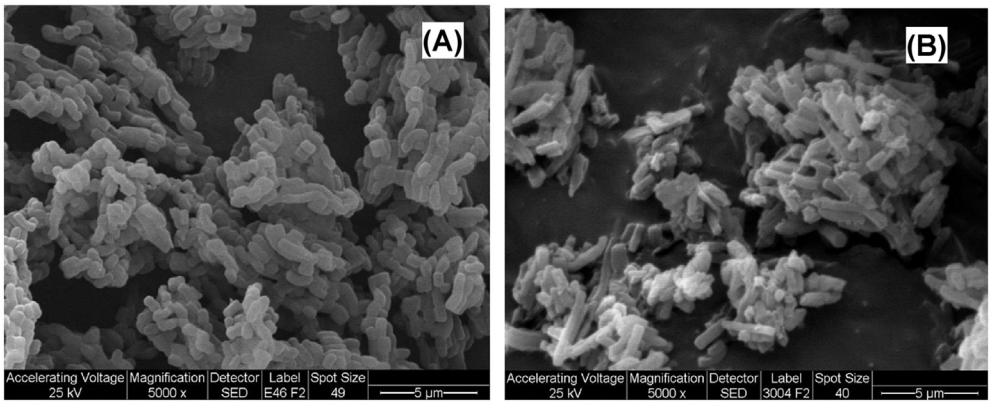

Fig. 2. SEM images: (A) SBA-15, (B) SBA-15(30).

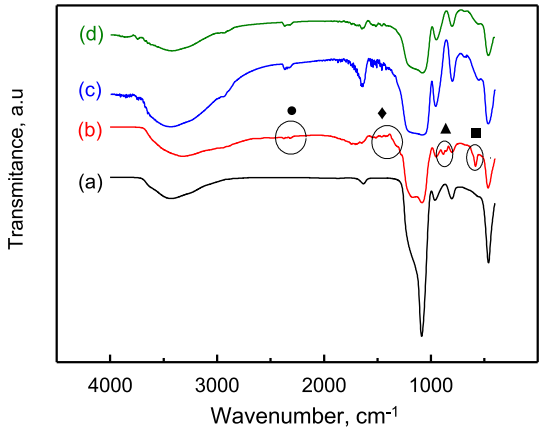

Fig. 3. FTIR spectra: (a) SBA-15, (b) SBA-15(30), (c) SBA-15(20), (d) SBA-15(10). C–O–C vibrations (◆), C–S vibrations (■), S–O vibrations (▲) and SH group vibrations (●).

Table 2
Surface chemical composition (atomic concentration %) obtained by XPS.

Sample	%C	%O	%Si	%S	$\%S_{merc}$	$\%S_{sulf}$
SBA-15	1.65	65.4	32.9	–		
SBA-15(30)	11.50	58.0	25.8	4.7	9.0	91.0
SBA-15(20)	14.30	56.2	27.7	1.8	39.4	60.6
SBA-15(10)	16.20	54.5	26.9	2.4	69.0	31.0

%Smerc and %Ssulf corresponds to sulfur associated to propyl-SH and propyl-SO_3H groups respectively.

oxygen on its surface. The percentage of carbon detected may be due to residues of the copolymer used as template during the synthesis. The low carbon content in this sample indicates the effectiveness of the copolymer removal by calcination.

Effective functionalization takes place in the samples SBA-15(X), since the %C was increased due to the presence of propyl groups, and also sulfur was detected on their surface. An estimation of the content of template can be performed with the results of XPS in the functionalized samples. Each functional group attached to the surface has an atomic relation C/S = 3, therefore knowing the sulfur content, the %C associated with those functional groups can be calculated. The difference with the total %C is the corresponding to residues from the template. In this way, a residue of 6.2%C in the sample SBA-15(30) was estimated, while in samples SBA-15(20) and SBA-15(10) the residue was 12.3%C and 13.5%C respectively. On the other hand, the percentages of sulfur in the samples indicate that the incorporation of functional groups was slightly higher for the SBA-15(30) sample. These are very interesting results. It can be noted that the amount of non-removed template decreases as the hydrogen peroxide concentration used during mercapto groups oxidation increases. This suggests that even thought the ethanol does not remove all the template, a fraction of this is then oxidized by H_2O_2, and the higher its concentration, the higher the amount of template removed.

With this technique, information about the degree of oxidation achieved in each sample can be obtained analyzing the XPS signals for sulfur. Fig. 4 shows XPS spectra of the S 2*p* signal corresponding to the functionalized samples. Two oxidation states of sulfur (S^{6+} and S^{2-}) were observed, ascribed to the simultaneous presence of sulfonic (S 2*p*3/2 at 169 eV) and mercapto (S 2*p*3/2 at 163.8 eV) groups [81–83]. The percentages of both types of sulfur are shown in Table 2, indicating that the 91% of the functional groups were effectively oxidized during the preparation of sample SBA-15(30). This is consistent with the hardly visible signal corresponding to the SH vibration at 2400 cm^{-1} in the FTIR spectra (Fig. 3, curve b). The XPS results for the samples SBA-15(20) and SBA-15(10) indicated that the degree of oxidation is improved as the concentration of H_2O_2 in the preparation increases. Also, the presence of more thiol groups was observed by FTIR in these samples. Using the results summarized in Table 2, it is possible to estimate the density of sulfonic groups in each catalyst, resulting to be 3.65, 0.81, and 0.53 µmol m^{-2} for the SBA-15(30), SBA-15(20), and SBA-15(10) respectively.

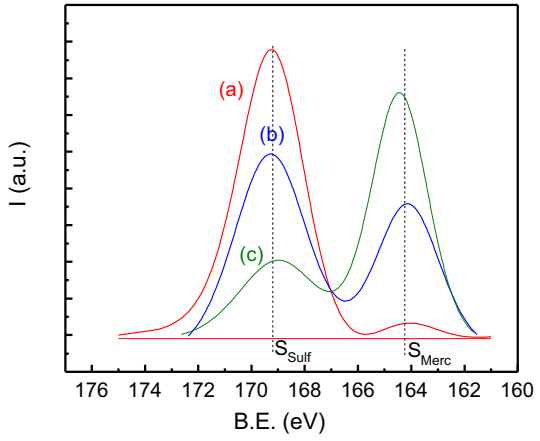

Fig. 4. XPS spectra of the S 2*p* signal corresponding to the samples: (a) SBA-15(30), (b) SBA-15(20) and (c) SBA-15(10).

3.1.5. Potentiometric titration

The functionalization of the surface of the catalyst was verified by FTIR and XPS, however it is also necessary to investigate the strength and amount of acid sites obtained in the catalysts.

Fig. 5 shows the potentiometric titration curves of the functionalized samples. It has been previously shown that the SBA-15 support has no acidity, or very low amount of weak acid sites [32,49]. A higher value of initial potential in the titration curve of the sample SBA-15(30) indicates an appreciable strength of the sulfonic acid groups. A total amount of acid sites of 1.8 mmol g^{-1} was detected for this sample, as determined by the inflection point of the curve. Taking into account the BET surface, the acid sites density results to be 4.92 μmol m^{-2}. For the samples SBA-15(20) and SBA-15(10) the acidity detected was 0.51 mmol g^{-1} (1.2 μmol m^{-2}) and 0.19 mmol g^{-1} (0.43 μmol m^{-2}) respectively. These values, obtained with a completely independent analytical technique, are in very good agreement with the values of acid sites density calculated using the XPS and BET results, presented in Section 3.1.4. J.P. Lourenço et al. [71], employing the one-step procedure [60] synthesized these materials with an amount of acid sites ranged between 0.54 and 0.74 mmol g^{-1}, leading to a density of sites between 0.7 and 1 μmol m^{-2}, mainly due to the high surface area obtained (600–750 m^2 g^{-1}). The authors determined a pore size between 56 and 79 Å, higher than the values obtained in this work. The non-functionalized SBA-15 catalysts used by Oliveira et al. [37] had an acid sites density of 0.31 μmol m^{-2}, which is even lower than the acid sites density of the functionalized SBA-15(10) used in the present study.

It is important to highlight that the acid sites density obtained in the present work is almost 4 times higher that those previously reported [71].

3.1.6. Thermal stability

The thermal stability of the samples was studied by different techniques. Fig. 6A and B shows the results of TGA and TPD experiments for the fresh catalyst SBA-15(30). A significant decrease in weight occurs around 100 °C (Fig. 6A), which many authors attributed to the loss of physisorbed water in the material [60,71]. The FID detector is not responsive to water, but a maximum in the signal at 100 °C is observed in Fig. 6B, that shows the TPD results. Therefore, the decrease in weight is necessarily associated with carbon molecules that are desorbed from the surface when heated in nitrogen. These are moieties of the block copolymer that were not completely removed in the washing steps during the catalyst synthesis, and that were previously observed by XPS. It is also possible that if water is removed during heating, this helps the release of these compounds.

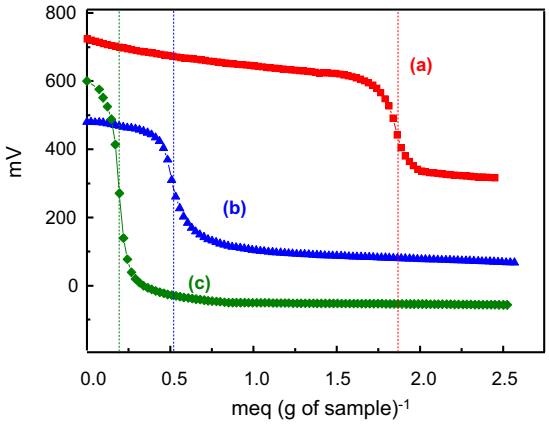

Fig. 5. Potentiometric titration with butylamine of samples: (a) SBA-15(30), (b) SBA-15(20) and (c) SBA-15(10).

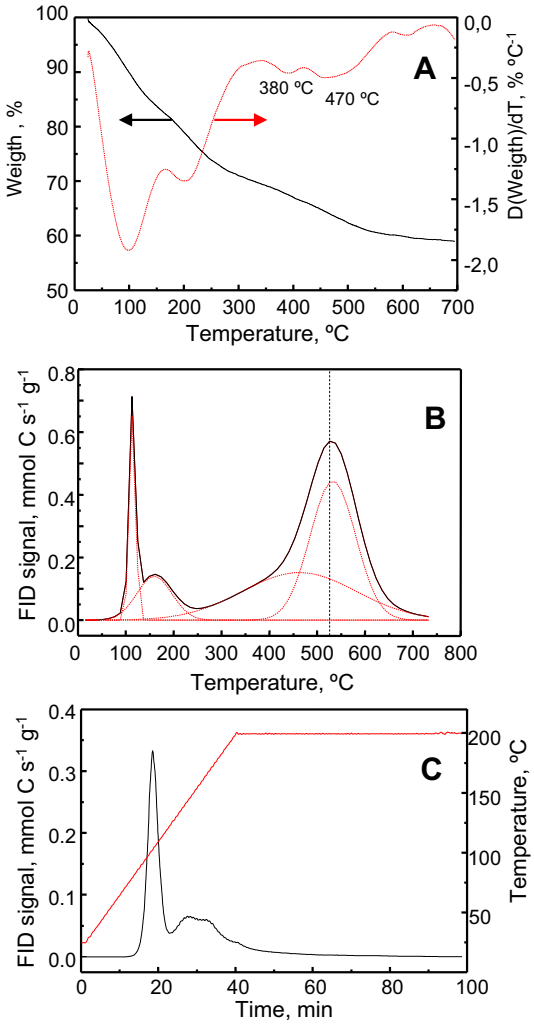

Fig. 6. **A**. TGA and DTG for sample SBA-15(30). **B**. N_2 TPD of sample SBA-15(30). **C**. TPD during N_2 treatment of sample SBA-15(30) before reaction.

The weight decrease between 300 °C and 600 °C is attributed to degradation of the propyl groups. DTG profile indicates two peaks with maxima at 380 °C and 470 °C, associated with the decomposition of propyl-SH and propyl-SO_3 groups respectively [60]. The loss of weight in the range 500–700 °C corresponds to decomposition of residues of the propylsulfonic acid.

The high sensitivity of the TPD technique used in this study allows to distinguish an area of decomposition, with a shoulder around 360–400 °C, which would indicate the presence of some propyl-SH groups, consistent with those observed by other authors. However, the presence of these non-oxidized groups was hardly visible in the IR spectrum of the sample (Fig. 3, curve b) and in the XPS spectra (Fig. 4). Moreover, the peak in the TPD profile at 520 °C corresponds certainly to the decomposition of the propyl-SO_3H acid groups, a substantially higher temperature than that observed by TGA. This indicates that the sample SBA-15(30) has mainly oxidized sites, with good thermal stability, better than those reported by other authors. However, according to the TPD profile (Fig. 6B), the loss of functional groups from 300 °C in N_2 stream can not be completely ruled out.

The presence of traces of the template could hinder access to the acid sites during the reaction. But, the treatment under N_2 at 200 °C performed previous to the reaction removes completely these residues, as shown in Fig. 6C for a typical pre-treatment experiment simulated outside the reactor. In the samples SBA-15(20) and SBA-15(10) the complete elimination of the residual template by the treatment with N_2 was also verified.

3.2. Activity results

3.2.1. Effect of acidity level in the catalyst

The three catalysts were tested in reaction operating at 300 °C and WHSV = 3.5 h^{-1}. Previously, a blank test was performed with pure silica SBA-15, which was catalytically inactive due the absence of acidity.

Fig. 7A shows the evolution of glycerol conversion with time on stream (TOS) obtained for the three catalysts. A decrease in the conversion with TOS was observed in all cases due to catalyst deactivation. The deactivation rate was similar for samples SBA-15(20) and SBA-15(10), and substantially lower for the SBA-15(30). The glycerol conversion reached with this sample was also higher than for the others, being this related to the higher number and density of acid sites. In fact, there is a correlation of the activity with the acid sites density and the amount of propyl-SO_3H groups present on the catalyst surface.

Significant differences were observed in the selectivity to acrolein (Fig. 7B), being practically constant and close to 80% for the sample SBA-15(30). For the samples SBA-15(20) and SBA-15(10) the selectivity drops from 70% to 30% with time on stream. This is because these two samples have few acid sites with enough strength for the production of acrolein, which are deactivated by coke deposition at low reaction times. The relatively low concentration of acid sites in these two catalysts, make them much more sensitive to the coke deposits, and even though a lower amount of coke can be expected in these materials, its toxicity is higher due to the lower initial availability of active sites. These results indicate that the non-oxidized thiol sites are not active for the reaction, because they did not show acidity as indicated by the potentiometric titration analyses.

To obtain more information about the degree of deactivation in each sample after 6 h in TOS, the used materials were studied by potentiometric titration (Fig. 8). Practically no acid sites were detected for samples SBA-15(20) and SBA-15(10), around 0.07 mmol g^{-1} in both cases. On the other hand, for sample SBA-15(30) at this reaction time 0.17 mmol g^{-1} of acid sites were available for the reaction.

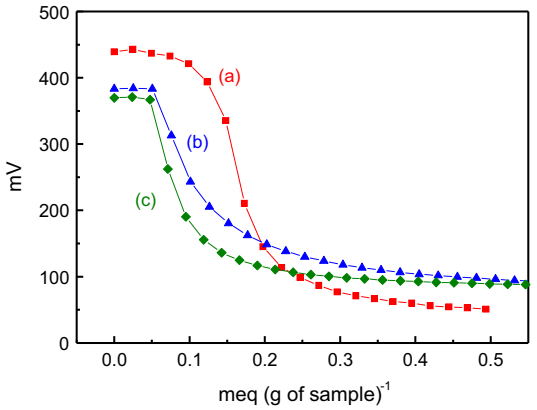

Fig. 8. Potentiometric titration with butylamine of samples: (a) SBA-15(30), (b) SBA-15(20) and (c) SBA-15(10) after reaction. T = 300 °C, WHSV = 3.5 h^{-1} and TOS = 6 h.

3.2.2. Effect of temperature

The sample SBA-15(30) was tested at different reaction temperatures, between 275 °C and 350 °C, operating at a glycerol WHSV = 3.5 h^{-1}.

Fig. 9A shows the evolution of glycerol conversion with time on stream (TOS) obtained for this catalyst. The reaction temperature had significant effect on glycerol conversion. The initial conversion (at 0.5 h TOS) was 98% at 350 °C, while at 275 °C it only reached 62%.

A decrease in the conversion with TOS was observed at all the temperatures studied, being the deactivation rate significantly affected by temperature. It can be seen that at 350 °C the fastest deactivation occurred, and this phenomenon was attenuated when the reaction was carried out at 300 °C. The better stability was achieved at intermediates temperatures; in the range of 300–325 °C. The conversions obtained at 6 h TOS, were 54% and 45% at 325 and 300 °C, respectively. A significant improvement respect to 275 °C (32%) was obtained. However, a further increment of temperature to 350 °C was detrimental, being the conversion at 6 h only 20%.

To understand the deactivation phenomena, a brief review of the reaction mechanism is necessary. The glycerol dehydration on acid catalysts occurs following two distinct pathways: the removal of one of the primary hydroxyl groups from the terminals carbons in the glycerol molecule, leading to hydroxy-acetone (acetol); and simultaneously the dehydration of the secondary OH group from the central carbon, producing 3-hydroxypropanal (an unstable product) which is subsequently dehydrated to acrolein.

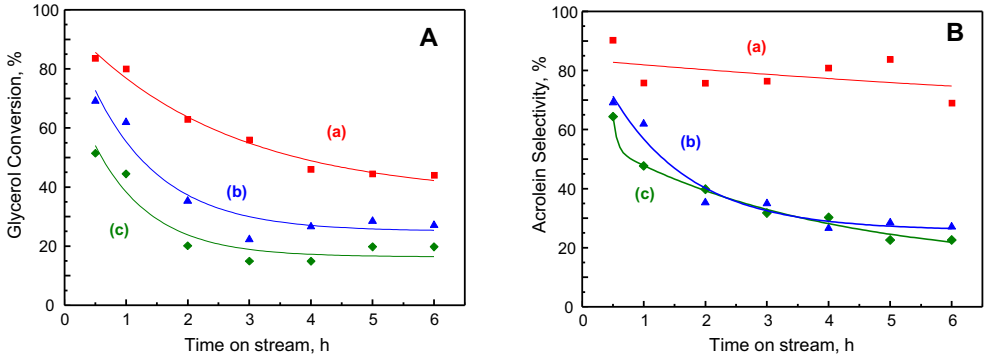

Fig. 7. Glycerol conversion **(A)** and acrolein selectivity **(B)** with time on stream for samples SBA-15(30) (■), SBA-15(20) (▲) and SBA-15(10) (♦). WHSV = 3.5 h^{-1} and T = 300 °C.

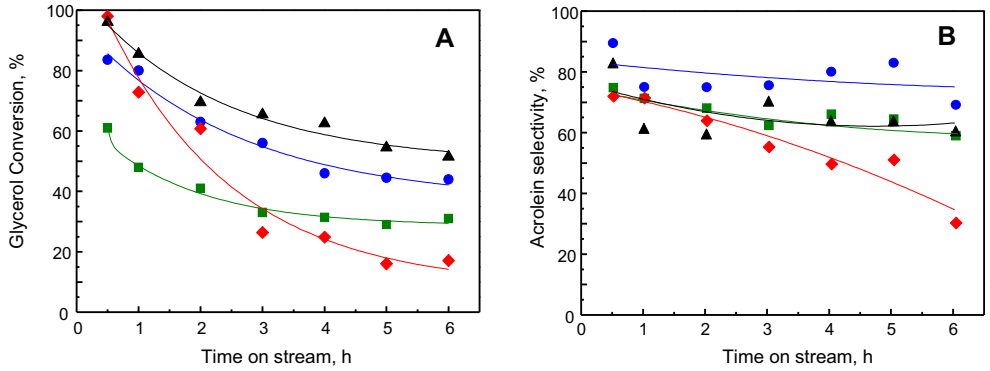

Fig. 9. Glycerol conversion **(A)** and acrolein selectivity **(B)** with time on stream for SBA-15(30) catalyst at WHSV = 3.5 h^{-1} and different temperatures: 275 °C (■), 300 °C (●), 325 °C (▲), 350 °C (♦).

The main product obtained with the SBA-15(X) catalysts was acrolein, due to the presence of Brønsted acid sites on the surface and in correlation with the mechanism previously suggested [34,37]. Acetol, propanal, acetaldehyde, and non-identified products ("others") with high molecular weight were detected. The route of formation of these compounds is through the acrolein, which is highly reactive and can undergo secondary reactions. Acrolein itself could be converted to many heavier products including higher aldehydes, olefins, heterocyclic and/or aromatic compounds by a complex reaction network including the reductive coupling, aldol condensation, Diels–Alder reaction, dehydration, and dehydrogenation as well as hydrogenation [25]. A.B. Sherrill et al. studied the reactions of acrolein on TiO_2, observing two carbon-carbon bond forming reactions: reductive coupling to form olefins and condensation of two acrolein molecules to give a C_6H_8O product (2-methyl-2,4-pentanedial) [84]. Also, a secondary hydrogenation reaction of the acrolein can lead to the formation of allyl alcohol [25], and then heterocyclic compounds can be formed from this alcohol [85].

All these products are responsible for coke formation and catalyst deactivation, and are cyclic unsaturated and oxygenated compounds like phenol, dihydrofuran, cyclopentenone and cyclohexenone.

Fig. 9B shows the selectivity to acrolein with TOS at different temperatures. The catalyst was more selective to acrolein when reacted at 300 °C, with a nearly constant selectivity of approximately 80%. This selectivity is higher than values previously reported, that were in the order of 60% [32]. The results at 275 °C and 325 °C were also good, with selectivities of approximately 70%. On the other hand, there was a marked decrease in selectivity with time on stream at 350 °C, to below 40% at 6 h. The deactivation at 350 °C could be due to a transformation of acrolein into heavy compounds, leading to a fast deposition of coke. However, a monotonic increment of the concentration of "others" with TOS was not observed (not shown), being practically constant as a function of time on stream.

An increment of the production of acetaldehyde was observed at 350 °C. This compound is also responsible for the production of coke [86].

The other possibility is that at 350 °C the acid groups decomposed, thus decreasing the number of acid sites.

To separate the effects of deactivation by coke deposition and by active site loss, quantification of acid sites in the fresh SBA-15(30) material was performed by potentiometric titration of a sample treated in N_2 at 325 °C during 6 h Fig. 10 shows that as a result of this treatment, the acidity decreased to 0.45 mmol g^{-1} in the material, indicating that at 325 °C approximately 75% of the active sites

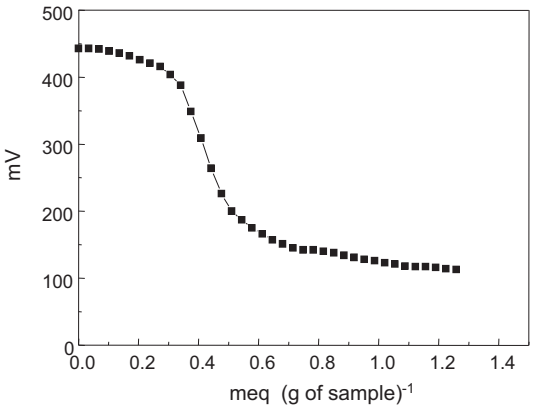

Fig. 10. Potentiometric titration with butylamine of sample SBA-15(30) after treatment in N_2 at 325 °C during 6 h.

were lost. Similar results were obtained for the catalyst treated at 300 °C. However, at 350 °C the loss of acid sites was more important (not shown). Therefore, the main deactivation phenomenon in these materials at temperatures above 300 °C was the loss of acid sites just by a thermal mechanism. In this mechanism the propylsulfonic group decomposes, thus decreasing the number of active sites. As indicated in Fig. 10 (compare with Fig. 5, curve a) there is a major loss of acid groups just due to a treatment at 300 °C. In this sense, it is therefore important to point out that this deactivation mechanism is irreversible. Propyl sulfonic functional groups may be lost by hydrolysis, as was reported in the acetylation reaction of glycerol [87]. But the dehydration of glycerol studied in this work is done in gas phase, therefore that possibility is ruled out.

In terms of yield to acrolein, the most favourable temperature to operate was 300 °C, obtaining a high selectivity.

3.2.3. *Effect of space velocity*

To analyze the effect of space velocity, temperature was set at 300 °C, at which the best catalyst performance was obtained. Fig. 11 shows an improvement in the conversion at a space velocity of WHSV = 1 h^{-1} as compared to the results obtained at WHSV = 3.5 h^{-1}, which is a logic result. However, it is interesting that the conversion as a function of time under both conditions decreased at a similar rate, in spite of the different conversions. This suggests that either the coke is formed at the same rate from the glycerol and the products or there is a lost of active sites due to thermal decomposition, as suggested by the TPD profiles shown in

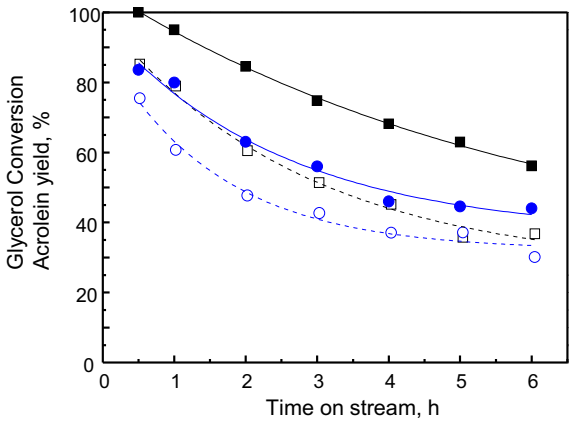

Fig. 11. Glycerol conversion (full symbol) and Acrolein yield (empty symbol) at T = 300 °C and different WHSV: 3.5 h^{-1} (●, ○), 1 h^{-1} (■, □).

Fig. 6B. In this sense, it is important to take into account that glycerol forms oligomers which may lead to coking reactions and the same mechanism is applicable to acetol [88].

At the lower space velocity the selectivity was higher, and in order to maximize acrolein yield, it is convenient to operate in this condition.

The stability obtained operating at WHSV = 1 h^{-1} is much lower than that reported by Lourenço et al. [71. An important difference is that in the catalyst used in the present work the density of acid sites is 5 times higher, and this explains the faster deactivation. However, the samples SBA-15(20) and SBA-15(10) which have less density of acid sites showed similar results regarding the stability. Therefore the main cause of the lower stability in these catalysts can be the smaller pore size obtained in the synthesis, in comparison to the values reported by Lourenço et al. [71].

3.3. Analysis of deactivated catalyst

3.3.1. Potentiometric titration and TPO after reaction

To analyze the level of deactivation of the catalyst at different operating conditions, the amount of acid sites available after reaction was evaluated. Fig. 12 shows the potentiometric titration results for the used samples. A significant catalyst deactivation due to coke deposition on the active sites occurs, and the amount of available acid sites is significantly lower in comparison with the fresh sample (Fig. 5a). After the reactions at 275 °C and 300 °C, similar titration profiles were obtained, and less than 0.2 mmol g^{-1} of acid sites were detected, being 1.8 mmol g^{-1} in the fresh sample, and 0.45 mmol g^{-1} after a thermal treatment both at 325 °C and 300 °C. The lower acidity detected with this technique in the catalyst used at 325 °C in the reaction as compared to the catalyst treated at the same temperature under an inert gas flow (Fig. 10), indicates that the deactivation proceeds both by coke deposition and active sites lost. The amount of acid sites observed with this technique in the solid deactivated at 350 °C was very low.

The TPO profiles and coke content were similar in all cases. Fig. 13 shows the results for the catalyst deactivated at 325 °C (b), and the TPO of the fresh material (a), detecting 24% C that corresponds to coke deposited during reaction. Furthermore, since the amount of available acid sites detected after the reaction is lower than that obtained after an equivalent thermal treatment, it is evident that the deactivation in this catalyst involves both a loss of active sites and coke deposition.

4. Conclusions

The glycerol dehydration was studied using SBA-15 materials functionalized with propyl sulfonic acids groups on its surface. The prepared catalyst showed a BET area of 366 m^2 g^{-1} with 32 Å of pore size and an acidity of 1.8 mmol g^{-1}. It was active for the glycerol dehydration and highly selective to acrolein, reaching the best yield operating at 300 °C. The deactivation of the catalyst was produced by coke deposition and active site loss due to thermal decomposition. The routes of coke formation were from acrolein and from glycerol, due to oligomerization and condensation reactions. The high acid sites density of the material favoured this deactivation mechanism. However, the reaction temperature played an important role, because of the thermal stability of the functional groups. Temperatures above 300 °C were detrimental for the operation with these materials and led to an irreversible deactivation. This phenomenon may be a major problem for a large scale application of these types of catalysts in this reaction.

The results reported in this work evidence that with optimized experimental conditions, a catalytic system with a high performance can be achieved. The benefits of hierarchical pores on enhancing the apparent activity and selectivity of the catalysts have been verified. In this sense, previous mesoporous catalysts had shown acrolein selectivities lower than 60% [32]. In this work, the SBA-15(30) catalyst improved the selectivity but the stability was only slightly higher than that obtained with microporous materials. The catalysts regeneration seems to be difficult to perform by

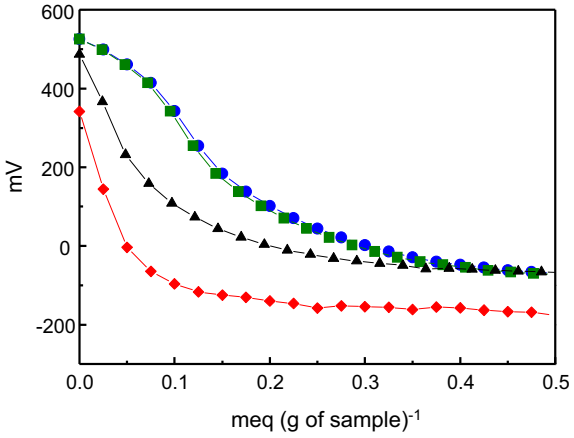

Fig. 12. Potentiometric titration with butylamine of sample SBA-15(30) deactivated at different temperatures: 275 °C (■), 300 °C (●), 325 °C (▲), 350 °C (♦).

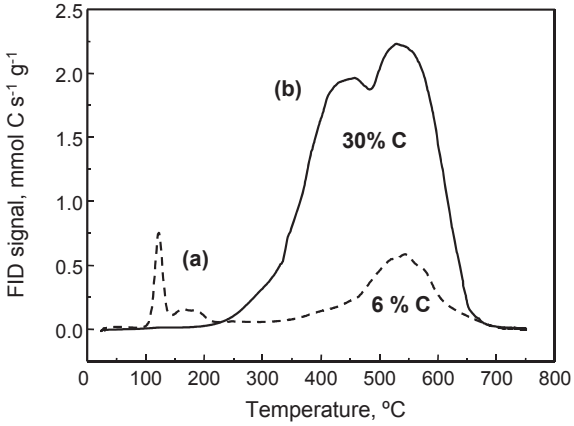

Fig. 13. TPO profiles for SBA-15(30) catalyst before (a) and after reaction at 325 °C (b).

conventional treatments such as oxidation in air, and may require additional studies using other alternatives, such as solvent extraction.

Acknowledgements

The authors acknowledge the financial support received from ANPCyT (PICT 2013, No1252), UNL (PACT 69) and CONICET (PIO YPF-CONICET, 13320130100209CO, 2013). Thanks are also given to ANPCyT for the purchase of the SPECS multitechnique analysis instrument (PME8-2003), and to Lic. María Fernanda Mori for their assistance in technical interpretation of XPS spectra.

References

[1] G. Knothe, J. Krahl, J.V. Gerpen, The Biodiesel Handbook, AOCS Press, Champaing, IL, 2005.
[2] M. Ayoub, A.Z. Abdullah, Renew. Sust. Energy Rev. 16 (2012) 2671–2686.
[3] M.D. González, Y. Cesteros, J. Llorca, P. Salagre, J. Catal. 290 (2012) 202–209.
[4] M.D. González, P. Salagre, R. Mokaya, Y. Cesteros, Catal. Today 227 (2014) 171–178.
[5] L. Liu, B. Wang, Y. Du, Z. Zhong, A. Borgna, Appl. Catal. B (2015) 1–12.
[6] C.H. Zhou, H. Zhao, D.S. Tong, L.M. Wu, W.H. Yu, Catal. Rev. 55 (2013) 369–453.
[7] J. Pérez-Pariente, I. Dıaz, F. Mohino, E. Sastre, Appl. Catal. A 254 (2003) 173–188.
[8] C. Márquez-Alvarez, E. Sastre, J. Pérez-Pariente, Top. Catal. 27 (2004) 105–117.
[9] I. Díaz, F. Mohino, T. Blasco, E. Sastre, J. Pérez-Pariente, Microporous Mesoporous Mater. 80 (2005) 33–42.
[10] J.A. Cecilia, C. García-Sancho, J.M. Mérida-Robles, J. Santamaría-González, R. Moreno-Tost, P. Maireles-Torres, Catal. Today 254 (2015) 43–52.
[11] S.S. Priya, V.P. Kumar, M.L. Kantam, S.K. Bhargava, A. Srikanth, K.V.R. Chary, Ind. Eng. Chem. Res. 54 (2015) 9104–9115.
[12] A. Corma, S. Iborra, A. Velty, Chem. Rev. 107 (2007) 2411–2501.
[13] M. Pagliaro, R. Ciriminna, H. Kimura, M. Rossi, C. DellaPina, Angew. Chem. Int. Ed. 46 (2007) 4434–4440.
[14] C. Zhou, J.N. Beltramini, Y. Fan, G.Q. Lu, Chem. Soc. Rev. 37 (2008) 527–549.
[15] Y. Zheng, X. Chen, Y. Shen, Chem. Rev. 108 (2008) 5253–5277.
[16] A. Behr, J. Eilting, K. Irawadi, J. Leschinski, F. Lindner, Green Chem. 10 (2008) 13–30.
[17] G.W. Huber, J.W. Shabaker, J.A. Dumesic, Science 300 (2003) 2075–2077.
[18] Y. Moro-Oka, W. Ueda, Adv. Catal. 40 (1994) 233–273.
[19] J.-L. Dubois, United State Patent 8378136 B2, Arkema, France, 2013.
[20] J. Deleplanque, J.-L. Dubois, J.-F. Devaux, W. Ueda, Catal. Today 157 (2010) 351–358.
[21] Y. Choi, D.S. Park, H.J. Yun, J. Baek, D. Yun, J. Yi, ChemSusChem. (2012) 2460–2468.
[22] X. Feng, Y. Yao, Q. Su, L. Zhao, W. Jiang, W. Ji, C.-T. Au, Appl. Catal. B 164 (2015) 31–39.
[23] F. Wang, J.L. Dubois, W. Ueda, J. Catal. 268 (2009) 260–267.
[24] F. Wang, J.L. Dubois, W. Ueda, Appl. Catal. A 376 (2010) 25–32.
[25] S.H. Chai, H.P. Wang, Y. Liang, B.Q. Xu, Green Chem. 9 (2007) 1130–1136.
[26] F. Cavani, S. Guidetti, L. Marinelli, M. Piccinini, E. Ghedini, M. Signoretto, Appl. Catal. B 100 (2010) 197–204.
[27] L.Z. Tao, S.H. Chai, Y. Zuo, W.T. Zheng, Y. Liang, B.Q. Xu, Catal. Today 158 (2010) 310–316.
[28] C. García-Sancho, J.A. Cecilia, A. Moreno-Ruiz, J.M. Mérida-Robles, J. Santamaría-González, R. Moreno-Tost, P. Maireles-Torres, Appl. Catal. B 179 (2015) 139–149.
[29] A. Alhanash, E.F. Kozhevnikova, I.V. Kozhevnikov, Appl. Catal. A 378 (2010) 11–18.
[30] B. Katryniok, S. Paul, M. Capron, C. Lancelot, V. Bellière-Beca, P. Rey, F. Dumeignil, Green Chem. 12 (2010) 1922–1925.
[31] I. Martinuzzi, Y. Azizi, O. Zahraa, J.P. Leclerc, Chem. Eng. Sci. 134 (2015) 663–670.
[32] Y. Choi, H. Park, Y.S. Yun, J. Yi, ChemSusChem 7 (2014) 974–980.
[33] Y.T. Kim, K.D. Jung, E.D. Park, Microporous Mesoporous Mater. 131 (2010) 28–36.
[34] C.J. Jia, Y. Liu, W. Schmidt, A.H. Lu, F. Schüth, J. Catal. 269 (2010) 71–79.
[35] H.P. Decolatti, B.O. Dalla Costa, C.A. Querini, Microporous Mesoporous Mater. 204 (2015) 180–189.
[36] W.Y. Pan, L. Huang, F. Qin, Y. Zhuang, X.M. Li, J.X. Ma, W. Shen, H.L. Xu, Acta Phys. Chim. Sin. 31 (2015) 965–972.
[37] A.S. de Oliveira, S.J.S. Vasconcelos, J.R. de Sousa, F.F. de Sousa, J.M. Filho, A.C. Oliveira, Chem. Eng. J. 168 (2011) 765–774.
[38] H. Atia, U. Armbruster, A. Martin, Appl. Catal. A 393 (2011) 331–339.
[39] C.L. Lima, S.J.S. Vasconcelos, J.M. Filho, B.C. Neto, M.G.C. Rocha, P. Bargiela, A.C. Oliveira, Appl. Catal. A 399 (2011) 50–62.
[40] D. Stosic, S. Bennici, J.-L. Couturier, J.-L. Dubois, A. Auroux, Catal. Commun. 17 (2012) 23–28.
[41] B. Katryniok, S. Paul, V. Bellière-Baca, P. Rey, F. Dumeignil, Green Chem. 12 (2010) 2079–2098.
[42] K. Pathak, K.M. Reddy, N.N. Bakhshi, A.K. Dalai, Appl. Catal. A 372 (2010) 224–238.
[43] E. Tsukuda, S. Sato, R. Takahashi, T. Sodesawa, Catal. Commun. 8 (2007) 1349–1353.
[44] J.A. Melero, L.F. Bautista, G. Morales, J. Iglesias, R. Sánchez-Vázquez, Chem. Eng. J. 161 (2010) 323–331.
[45] J.A. Melero, R. Van Grieken, G. Morales, Chem. Rev. 106 (2006) 3790–3812.
[46] J.A. Melero, R. Van Grieken, G. Morales, M. Paniagua, Energy Fuels 21 (2007) 1782–1991.
[47] S.S. Reddy, B.D. Raju, V.S. Kumar, A.H. Padmasri, S. Narayanan, K.S. Rama Rao, Catal. Commun. 8 (2007) 261–266.
[48] D. Srinivas, L. Saikia, Catal. Surv. Asia 12 (2008) 114–130.
[49] E.I. Basaldella, M.S. Legnoverde, I. Jiménez-Morales, E. Rodríguez-Castellón, B.O. Dalla Costa, C.A. Querini, Adsorption 17 (2011) 631–641.
[50] K.A. Shah, J.K. Parikh, K.C. Maheria, Catal. Today 237 (2014) 29–37.
[51] S. Jeenpadiphat, E.M. Björk, M. Odén, D.N. Tungasmita, J. Mol. Catal. A 410 (2015) 253–259.
[52] G.M. Ziarani, N. Lashgari, A. Badiei, J. Mol. Catal. A 397 (2015) 166–191.
[53] X. Feng, G.E. Fryxell, L.Q. Wang, A.Y. Kim, J. Liu, K.M. Kemner, Science 276 (1997) 923.
[54] A.M. Liu, K. Hidajat, S. Kawi, D.Y. Zhao, Chem. Commun. (2000) 1145–1146.
[55] W.M. Van Rhijn, D.E. De Vos, B.F. Sels, W.D. Bossaert, P.A. Jacobs, Chem. Commun. (1998) 317–318.
[56] D. Das, J.F. Lee, S.F. Cheng, Chem. Commun. (2001) 2178–2179.
[57] Q.H. Yang, H. Liu, H. Yang, L. Zhang, Z.C. Feng, J. Zhang, C. Li, Microporous Mesoporous Mater. 77 (2005) 257.
[58] I.K. Mbaraka, D.R. Radu, V.S.Y. Lin, B.H. Shanks, J. Catal. 219 (2003) 329–336.
[59] M.H. Lim, C.F. Blanford, A. Stein, Chem. Mater. 10 (1998) 467–470.
[60] D. Margolese, J.A. Melero, S.C. Christiansen, B.F. Chmelka, G.D. Stucky, Chem. Mater 12 (2000) 2448–2459.
[61] J.A. Melero, G.D. Stucky, R. Van Grieken, G. Morales, J. Mater. Chem. 12 (2002) 1664–1670.
[62] S. Hamoudi, S. Kaliaguine, Microporous Mesoporous Mater. 59 (2003) 195–204.
[63] S. Hamoudi, S. Royer, S. Kaliaguine, Microporous Mesoporous Mater. 71 (2004) 17–25.
[64] D. Zhao, Q. Huo, J. Feng, B.H. Chmelka, G.D. Stucky, J. Am. Chem. Soc. 120 (1998) 6024–6036.
[65] A.P. Wight, M.E. Davis, Chem. Rev. 102 (2002) 3589–3614.
[66] D.M. Ford, E.E. Simanek, D.F. Shantz, Nanotechnology 16 (2005) 458–475.
[67] H. Yoshitake, J. Chem. 29 (2005) 1107–1117.
[68] W.D. Bossaert, D.E. DeVos, W.M. VanRhijn, J. Bullen, P.J. Grobet, P.A. Jacobs, J. Catal. 182 (1999) 156–164.
[69] K. Niknam, D. Saberi, M.N. Sefat, Tetrahedron Lett. 50 (2009) 4058–4062.
[70] S.C. Fung, C.A. Querini, J. Catal. 138 (1992) 240–254.
[71] J.P. Lourenço, M.I. Macedo, A. Fernandes, Catal. Commun. 19 (2012) 105–109.
[72] M.L. Pisarello, B.O. Dalla Costa, N.S. Veizaga, C.A. Querini, Ind. Eng. Chem. Res. 49 (2010) 8935–8941.
[73] K.S.W. Sing, D.H. Everett, R.A.W. Haul, L. Moscou, R.A. Pierotti, J. Rouquerol, T. Siemieniewska, Pure Appl. Chem. 57 (1985) 603–619.
[74] S. Lowell, J.E. Shields, M.A. Thomas, M. Thommes, Characterization of Porous Solids and Powders: Surface Area, Pore Size and Density, Kluwer Academic Publishers, 2003.
[75] L. Sarkisov, P.A. Monson, Langmuir 17 (2001) 7600–7604.
[76] Chia-Hung Lee, Tien-Sung Lin, Chung-Yuan Mou, Nano Today 4 (2009) 165–179.
[77] S. Ruthstein, J. Schmidt, E. Kesselman, Y. Talmon, D. Goldfarb, J. Am. Chem. Soc. 128 (2006) 3366–3374.
[78] I. Izquierdo-Barba, M. Colilla, M. Manzano, M. Vallet-Regí, Microporous Mesoporous Mater. 132 (2010) 442–452.
[79] G. Sartori, F. Bigi, R. Maggi, R. Sartorio, D.J. Macquarrie, M. Lenarda, L. Storaro, S. Coluccia, G. Martra, J. Catal. 222 (2004) 410–418.
[80] B. Stuart, Infrared Spectroscopy: Fundamentals and Applications, Wiley, New York, 2004.
[81] A.J. Crisci, M.H. Tucker, M.-Y. Lee, S.G. Jang, J.A. Dumesic, S.L. Scott, ACS Catal. 1 (2011) 719–728.
[82] S.D. Evans, K.E. Goppert-Beraducci, E. Urankar, L.J. Gerenser, A. Ulman, S.G. Snyder, Langmuir 7 (1991) 2700–2709.
[83] N. Samarendra, N. Dutta, D.C. Frost, Fuel 62 (1983) 840–841.
[84] A.B. Sherrill, H. Idriss, M.A. Barteau, J.G. Chen, Catal. Today 85 (2003) 321–331.
[85] C.P. Bezouhanova, C.V. Titorenkova, C. Chanev, J. Mol. Catal. A Chem. 132 (1998) 87–90.
[86] A.G. Gayubo, A.T. Aguayo, A. Atutxa, R. Aguado, J. Bilbao, Ind. Eng. Chem. Res. 43 (2004) 2610–2618.
[87] I. Kim, J. Kim, D. Lee, Appl. Catal. B 148–149 (2014) 295–303.
[88] J. Barrault, J.M. Clacens, Y. Pouilloux, Top. Catal. 27 (2004) 137–142.